Evaluation of ^{18}F-UCB-H as a Novel PET Tracer for Synaptic Vesicle Protein 2A in the Brain

Geoffrey I. Warnock[1], Joël Aerts[1], Mohamed Ali Bahri[1], Florian Bretin[1], Christian Lemaire[1], Fabrice Giacomelli[1], Frederic Mievis[1], Nathalie Mestdagh[2], Tim Buchanan[2], Anne Valade[2], Joël Mercier[2], Martyn Wood[2], Michel Gillard[2], Alain Seret[1], André Luxen[1], Eric Salmon[1], and Alain Plenevaux[1]

[1]*Cyclotron Research Centre, University of Liège, Liège, Belgium; and* [2]*UCB Pharma, Brussels, Belgium*

Synaptic vesicle protein 2 isoforms are critical for proper nervous system function and are involved in vesicle trafficking. The synaptic vesicle protein 2A (SV2A) isoform has been identified as the binding site of the antiepileptic levetiracetam (LEV), making it an interesting therapeutic target for epilepsy. ^{18}F-UCB-H is a novel PET imaging agent with a nanomolar affinity for human SV2A. **Methods:** Preclinical PET studies were performed with isoflurane-anesthetized rats. The arterial input function was measured with an arteriovenous shunt and a β-microprobe system. ^{18}F-UCB-H was injected intravenously (bolus of 140 ± 20 MBq). **Results:** Brain uptake of ^{18}F-UCB-H was high, matching the expected homogeneous distribution of SV2A. The distribution volume (V_t) for ^{18}F-UCB-H was calculated with Logan graphic analysis, and the effect of LEV pretreatment on V_t was measured. In control animals the whole-brain V_t was 9.76 ± 0.52 mL/cm^3 (mean ± SD; $n = 4$; test–retest), and the reproducibility in test–retest studies was 10.4% ± 6.5% (mean ± SD). The uptake of ^{18}F-UCB-H was dose dependently blocked by pretreatment with LEV (0.1–100 mg/kg intravenously). **Conclusion:** Our results indicated that ^{18}F-UCB-H is a suitable radiotracer for the imaging of SV2A in vivo. To our knowledge, this is the first PET tracer for the in vivo quantification of SV2A. The necessary steps for the implementation of ^{18}F-UCB-H production under good manufacturing practice conditions and the first human studies are being planned.

Key Words: SV2A; brain imaging; ^{18}F; microPET

J Nucl Med 2014; 55:1336–1341
DOI: 10.2967/jnumed.113.136143

Synaptic vesicles (SVs) are crucial to neurotransmission and, in turn, rely on SV proteins for efficient function. SV proteins exist in many isoforms and are widely distributed throughout the brain (*1*). Although the role of some SV proteins has been studied in great detail and their function is generally understood (*1,2*), other SV proteins require further study. The potential value of SV protein 2 (SV2) isoforms (*3–5*) as drug targets has renewed interest in these proteins. The antiepileptic drug levetiracetam (LEV) binds to SV2A (*6*), suggesting a role for SV2A in the pathology underlying certain forms of epilepsy. To our knowledge, no tracers for the in vivo imaging of SV2A have yet been described.

Received Dec. 12, 2013; revision accepted Apr. 21, 2014.
For correspondence or reprints contact: Alain Plenevaux, Cyclotron Research Centre, University of Liège, 4000 Liège, Belgium.
E-mail: Alain.Plenevaux@ulg.ac.be
Published online Jun. 16, 2014.

Three major isoforms of SV2 have been identified (*7,8*): SV2A, SV2B, and SV2C. SV2A has been demonstrated to be critical for proper nervous system function and to be involved in vesicle trafficking and calcium regulation in neurotransmission (*9*). SV2A is homogeneously distributed in the rodent brain (*7*), whereas other isoforms have discrete distributions suggesting specific functional roles (*8*). Reduced expression of SV2A and SV2B in areas of synaptic loss in temporal lobe epilepsy and a selective increase in SV2C expression in sprouting mossy fibers in mesial temporal sclerosis have been reported (*4*), further indicating a role for SV2 in epilepsy and related neurodegeneration.

^{19}F-UCB-H is a novel ligand with a nanomolar affinity for SV2A and an in silico, in vitro, and in vivo ADME (absorption, distribution, metabolism, and excretion) profile that makes it suitable for consideration as a candidate SV2A PET ligand (*10*). A distribution coefficient of 2.3 suggests suitable membrane permeability (*10*), and preclinical dosimetry studies have already been reported (*11*). In the present study, we investigated the usefulness of ^{18}F-UCB-H as a tracer for SV2A in vivo using microPET in rats. Because of the absence of a suitable reference region devoid of SV2A, the use of reference region tracer kinetic models was precluded. To accurately quantify the uptake of ^{18}F-UCB-H in specific brain regions and to examine the reproducibility of tracer uptake in repeat studies, we measured the arterial input function (AIF) with a β-microprobe system (*12*); this approach made it possible to quantify the distribution volume (V_t) with the graphic analysis technique described by Logan et al. (*13*) (hereafter referred to as Logan graphic analysis).

MATERIALS AND METHODS

Animals

Male OFA (Oncins France strain A Sprague–Dawley) rats were initially obtained at 5 wk of age from Charles River Laboratories and subsequently bred at the University of Liège (BE-LA 2610359). The mean ± SD body weight at testing was 363 ± 115 g. The animals were housed under standard 12-h light:12-h dark conditions with food and water available ad libitum. All experimental procedures were approved by the Institutional Animal Care and Use Committee.

In Vitro Receptor Binding and Profiling

The affinity of ^{18}F-UCB-H for SV2 targets was assessed in vitro with previously described methods (*14*). In brief, membrane proteins (0.2–0.3 mg/assay) were incubated for 120 min at 4°C in 0.5 mL of 50 mM Tris–HCl buffer (pH 7.4) containing 2 mM $MgCl_2$, 1–2 nM LEV analog ^{3}H-ucb30889 {2*S*-2-[4-(3-azidophenyl)-2-oxo-1-pyrrolidinyl] butanamide; custom-synthesized by GE Healthcare}, and increasing concentrations of unlabeled competing drugs. ^{3}H-ucb30889 has a nanomolar

affinity for SV2A and high selectivity (*14*). Nonspecific binding was defined as the residual binding observed in the presence of 1 mM unlabeled LEV. At the end of the incubation period, the membrane-bound radioligand was recovered by rapid filtration through GF/C glass fiber filters presoaked in 0.1% polyethyleneimine and 1 mM LEV. The membranes were washed with 8 mL of ice-cold Tris buffer (pH 7.4). The total filtration procedure did not exceed 10 s/sample. The filters were dried, and the radioactivity was determined by liquid scintillation.

The affinity of ^{19}F-UCB-H for human and rat SV2A in both recombinant and native tissues was determined in competition binding experiments (performed at 37°C) with ^{3}H-ucb30889 (1,184 GBq/mmol). Selectivity profiling of ^{19}F-UCB-H (10 μM) against a panel of more than 55 targets was performed in-house or at CEREP (external subcontract). Standard binding or enzyme assay protocols were used with positive controls to validate the experiments. The dissociation kinetic rate constant for ^{19}F-UCB-H was determined by performing association kinetic analysis of ^{3}H-ucb30889 in the absence and presence of a concentration of ^{19}F-UCB-H that led to 60%–80% inhibition of radioligand binding at steady state. The combined datasets were analyzed by nonlinear regression as described by Motulsky and Mahan (*15*), with the assumption of a competitive interaction between ^{19}F-UCB-H and ^{3}H-ucb30889.

Radiochemistry and PET Studies

^{18}F-UCB-H was obtained in a 4-step radiosynthesis process (Fig. 1) involving nucleophilic labeling of a pyridine precursor, reductive amination of the labeled product, and internal cyclization. The major synthesis steps have been described elsewhere (*16,17*). ^{18}F-UCB-H was obtained from ^{18}F-F^{-} after 150 min at an overall radiochemical yield of 30% (uncorrected for decay), including purifications and formulation. The radiochemical purity was 97.1% ± 1.9%. The full radiochemical process will be described elsewhere.

All studies were performed under isoflurane anesthesia. ^{18}F-UCB-H was injected as a bolus via the femoral vein, and scans were performed with a Siemens/Concorde Focus 120 microPET scanner (*18*). To correct for attenuation, we performed a 10-min transmission scan with a ^{57}Co point source and an energy window of 120–125 keV (*18*). ^{18}F-UCB-H (140 ± 20 MBq; specific activity, 98.9 ± 68.7 GBq/μmol at injection; injected mass, 2.3 ± 6.9 μg) was injected after the transmission scan. An elevated dose of ^{18}F-UCB-H was injected to ensure a sufficient signal-to-noise ratio in β-microprobe counts. A high-dose PET detector normalization procedure was implemented to improve performance, and pilot studies confirmed that the PET detectors were not saturated at the dose injected. Emission data were then recorded for 60 min (30 × 2 s, 10 × 10 s, 6 × 30 s, 6 × 300 s, and 3 × 600 s) with an energy window of 350–650 keV and a coincidence-timing window of 6 ns.

Images were reconstructed with all corrections (except scatter (*18*)) by use of Fourier rebinning and filtered backprojection with a ramp filter cutoff at the Nyquist frequency. A total of 95 transaxial slices were obtained in a 256 × 256 matrix. The slice thickness was 0.796 mm, and the in-slice pixel size was 0.43 mm. Summed images (0–3 min) were used for automated coregistration to a standard rat brain template available in PMOD software (version 3.4; PMOD Technologies Ltd.); this step was followed by the application of atlas-based volumes of interest (also available in PMOD software). A subset of the full atlas-based volumes of interest, representing the widespread distribution of SV2A, was used for further analysis.

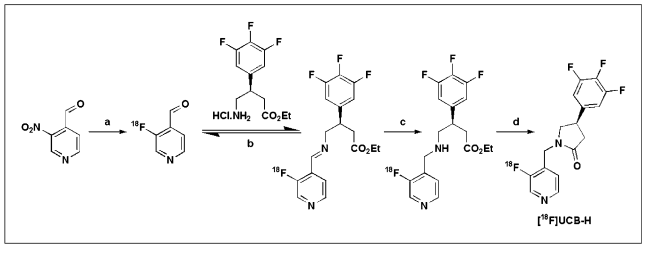

FIGURE 1. Overview of ^{18}F-UCB-H synthesis (*17*). Reagents and conditions: a = *N*-tetradecyltrimethylammonium^{+}^{18}F-F^{-}/tetraethylammonium^{+}HCO_3^{-} in dimethyl sulfoxide–*N*,*N*-dimethylformamide (*16*), 140°C, 2 min; b = triethylamine-methanol, 60°C, 20 min; c and d = $NaBH_4$, 60°C, 25 min. Et = ethyl group.

β-Microprobe System. A commercially available β-microprobe system (Swisstrace) was used for the measurement of blood activity as previously described (*12*). Placed in an arteriovenous shunt between the femoral artery and the femoral vein, the system allows the whole-blood AIF to be measured with a temporal resolution of 1 s and without blood loss. The physical characteristics of the system and probes have been described elsewhere (*19*). With data acquired in separate studies, the whole-blood AIF can be corrected for the plasma-to-whole blood ratio and for metabolism in vivo.

Shunt Apparatus and Surgery. A test–retest design was used for all studies. On test days, the animals were anesthetized with isoflurane, and polyethylene catheters (PE20; prefilled with heparinized saline at 50 U/mL) were implanted in the femoral artery and the femoral vein. The catheters were connected to an arteriovenous shunt driven by a peristaltic pump at 28.60 ± 0.18 mL/h. T connections in the shunt allowed intravenous injections and arterial blood sampling. After completion of the test (day 1) PET protocol, the catheters were removed, enrofloxacin (5 mg/kg subcutaneously) was administered to prevent infection, protamine (3 mg/kg intravenously) was administered to counteract the effects of heparin from the shunt system, a lidocaine spray (10 mg) was used to provide local analgesia, and the animals were allowed to recover. On the second test day, 1 wk later, arterial and venous catheters were implanted in the opposite leg for AIF measurement at retest.

On the first test day, pretreatment with vehicle (saline, 1 mL/kg intravenously) was performed. At retest, pretreatment with LEV (intravenous bolus of 0.1–100 mg/kg) or vehicle was performed. LEV was selected rather than unlabeled UCB-H to target specific binding without displacement of nonspecific binding. Blocking of ^{18}F-UCB-H by LEV was quantified by calculating the percentage change in the V_t as follows: $[(V_t^{retest} - V_t^{test})/V_t^{test}] \times 100$.

Blood Analysis. In a separate study to determine the correction factors for kinetic modeling, arterial blood samples (~400 μL for metabolite determination; ~100 μL for plasma-to-whole blood ratio) were taken every 10 s for the first minute and then at 1, 5, 10, 30, and 60 min (n = 3–5 for each time point) for correction from whole blood to plasma and for parent tracer fraction measurements. The sampling was staggered between animals such that no more than 1.5 mL of blood was taken from any animal. In LEV blocking studies, discrete samples (10 and 60 min) were taken to confirm that parent tracer and metabolite levels were in the same range as in the detailed study. Plasma was separated by centrifugation (1,100*g*, 5 min), and both plasma and whole blood were analyzed in a γ counter. For metabolite measurements, plasma proteins were removed with acetonitrile, and fractions were separated by high-performance liquid chromatography. Radioactive compounds were detected online, and counts were verified by γ counting. The plasma-to-whole blood ratio for ^{18}F-UCB-H was fitted with a 2-part spline-based model to accurately model rapid initial changes in distribution. This fitted curve was subsequently used to correct the whole-blood AIF. Similarly, a biexponential model was fitted to the measured fraction of the parent tracer over time, and the result was used to further correct the AIF for the metabolism of ^{18}F-UCB-H in vivo.

Kinetic Modeling

Time–activity curves were extracted from the brain volumes of interest and used in combination with the β-microprobe–derived AIF for kinetic modeling in PMOD software. The individually measured

AIF was corrected for the plasma-to-whole blood ratio and in vivo metabolism on the basis of the average ratio and parent fraction calculated previously, and the V_t was calculated with Logan graphic analysis (*13*). The start time of the linear section for the derivation of V_t was included as a parameter in the model fit. The start time ranged from 7.5 to 15 min. The model fit was optimized by including AIF delay in the model.

Statistics

The effect of LEV pretreatment on the V_t in test–retest studies was assessed with a 1-way ANOVA and then with the Tukey honestly significant difference test for post hoc comparisons by use of statistical package R (version 3.0.0; http://www.r-project.org/).

RESULTS

At 37°C, ^{19}F-UCB-H displayed a nanomolar (50% inhibitory concentration, 40 nM) affinity for recombinant human SV2A. A similar potency of ^{19}F-UCB-H for native SV2A was observed in rat and human brain (50% inhibitory concentration, 55 nM). ^{19}F-UCB-H rapidly dissociated from SV2A, with a half-life of less than 2 min.

As previously demonstrated (*10*), the in vitro ADME profile showed moderate clearance in rat and human microsomes, a marked ability to permeate CACO-2 cells, and no significant P-glycoprotein–mediated efflux. After a single intravenous administration in rats, ^{19}F-UCB-H showed rapid and high-level brain uptake, with a free brain-to-plasma ratio of greater than 1 at 5, 10, and 20 min after administration.

^{19}F-UCB-H was tested at 10 μM in radioligand binding assays against a panel of more than 55 targets, including receptors (adenosine, adrenergic, cannabinoid, dopamine, histamine, neurokinin, muscarinic, opioid, serotonergic, glycine, kainate, α-amino-3-hydroxy-5-methyl-4-isoxazolepropionic acid, and *N*-methly-D-aspartate), transporters (adenosine, noradrenaline, dopamine, serotonin, and γ-aminobutyric acid), ion channels (GABAA [γ-aminobutyric acid and benzodiazepine binding sites]), L-type and N-type calcium channels, ATP- and voltage-dependent potassium channels, tetrodotoxin-sensitive sodium channels, and human ether-a-go-go–related gene), and enzymes (acetylcholinesterase, cyclooxygenases 1 and 2, γ-aminobutyric acid transaminase, monoamine oxidases A and B, nitric oxide synthase, phospholipase A_2, and tyrosine hydroxylase). ^{19}F-UCB-H lacked activity (less than 50% effect or inhibition) for any of the targets.

The uptake of ^{18}F-UCB-H in the brain and spinal cord corresponded to the reported distribution of SV2A (Fig. 2), with widespread tracer uptake in the entire brain and clear uptake in the spinal cord visible within the field of view (full-size images not shown). Representative time–activity curves for the uptake of ^{18}F-UCB-H in the brain, combined with representative AIFs (uncorrected and corrected for plasma-to-whole blood ratio and in vivo metabolism), are shown in Figure 3. Brain uptake of ^{18}F-UCB-H after a bolus injection was rapid, without accumulation of the tracer in the brain over time. The biexponential fitted parent fraction curve used for the correction of the AIF is shown in Figure 4. The metabolism of ^{18}F-UCB-H in vivo was highly reproducible (SD range for parent fraction, 0.014–0.078).

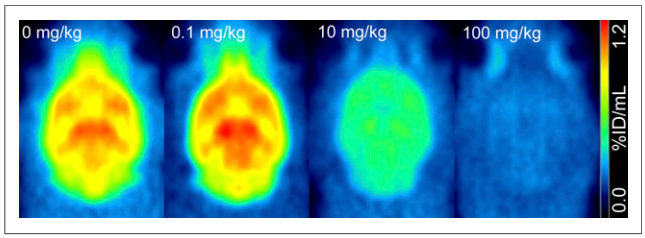

FIGURE 2. Brain uptake of ^{18}F-UCBH after blockade with successive doses of LEV (average uptake over 60 min). %ID = percentage injected dose.

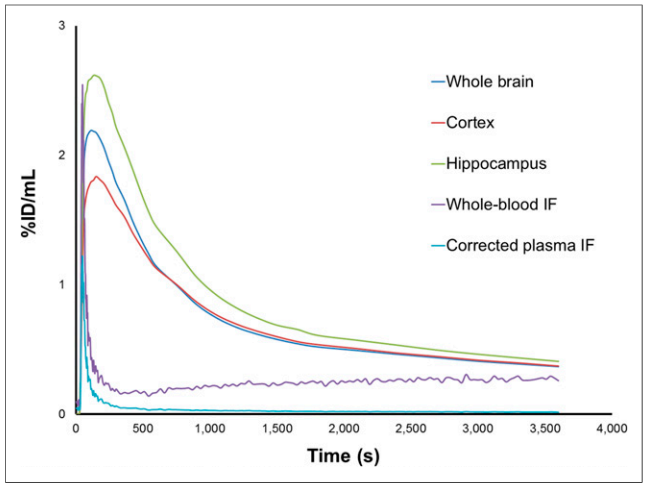

FIGURE 3. Time–activity curves for ^{18}F-UCBH uptake in representative regions, with β-microprobe–derived whole-blood input function (IF) and corrected AIF (corrected for plasma-to-whole blood ratio and plasma parent fraction with population-based corrections). %ID = percentage injected dose.

Logan graphic analysis of ^{18}F-UCB-H uptake in vehicle-treated animals was consistent and reproducible (start time, 7.5–15 min). An example of the model fit is shown in Figure 5. The V_t in the whole-brain volume of interest was 9.8 ± 0.5 mL/cm^3 (mean ± SD). The mean (n = 4; test–retest) V_t values in representative brain regions are shown in Table 1. The V_t was lowest in the pons (8.2 ± 0.3 mL/cm^3) and highest in the thalamus (12.1 ± 0.6 mL/cm^3). The whole-brain average variation in the V_t between test and retest scans was 10.4% ± 6.6% (Table 1). The highest degree of test–retest reproducibility was found in the medulla (variability, 9.4% ± 6.3%), and the lowest was found in the septum (14.9% ± 8.4%).

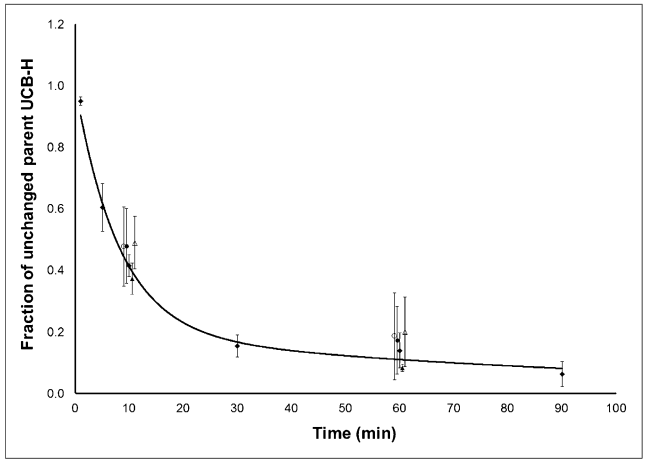

FIGURE 4. Parent fraction curve (♦; mean ± SD; n = 4; solid line represents biexponential fit) used for correction of AIF for tracer metabolism in vivo. Additional data points (jittered for legibility) show parent fraction after LEV pretreatment (n = 4 or 5 in each group; ○, 0.1 mg/kg; △, 1 mg/kg; ●, 10 mg/kg; ▲, 100 mg/kg).

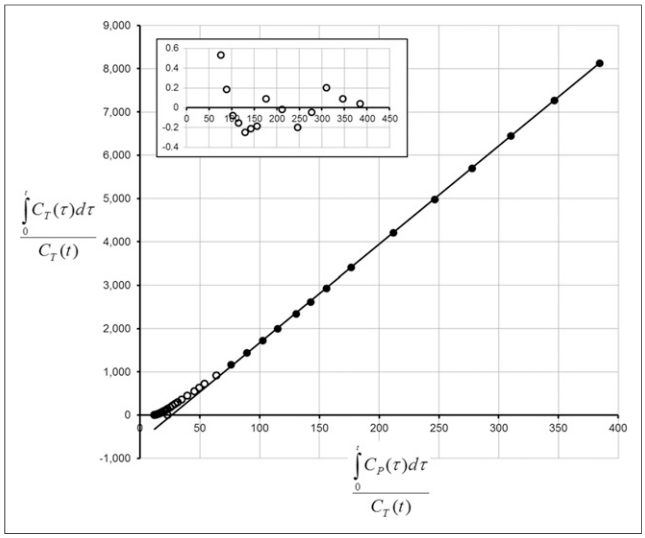

FIGURE 5. Example of Logan graphic analysis of ^{18}F-UCB-H binding in hippocampal region. Main plot: ○, data points excluded from fit; ●, data points included in fit; solid line represents fit. Subplot: fit residuals.

LEV pretreatment dose dependently reduced the V_t (greater percentage change in V_t) (Table 1) in all brain regions studied. The percentage changes in the V_t in the whole brain were 9.0%, 13.3%, 25.7%, and 43.8% at doses of 0.1, 1, 10, and 100 mg/kg ($n = 3$ or 4), respectively, and reached significance (1-way ANOVA: $F_{4,8} = 3.904$, $P = 0.048$; Tukey post hoc test, $P = 0.048$) at a dose of 100 mg/kg.

DISCUSSION

The goal of the present study was to evaluate the usefulness of the novel tracer ^{18}F-UCB-H for the in vivo quantification of SV2A before clinical use. Fully quantitative microPET was used, and the selectivity of ^{18}F-UCB-H for SV2A was tested with the antiepileptic LEV, which has been shown to directly target SV2A (*6*). Our results indicated that ^{18}F-UCB-H is a selective tracer for SV2A in vivo.

In vitro, ^{18}F-UCB-H was shown to have a high affinity and selectivity for SV2A. PET imaging of ^{18}F-UCB-H uptake (Fig. 2) revealed a high degree of tracer binding in the brain and spinal cord, consistent with the known distribution of SV2A (*7,8*). LEV was used to study selective binding of the tracer to SV2A. The high selectivity of LEV for SV2A was demonstrated in brain membranes and SVs from mice lacking SV2A (*6*), and a close analog of LEV, brivaracetam, also showed no binding to brain homogenates from SV2A knockout mice (*20*). Pretreatment with LEV in studies with a test–retest experimental design resulted in a dose-dependent reduction in the total V_t (Table 1), suggesting that the selectivity of ^{18}F-UCB-H for SV2A is conserved in vivo. As shown in Table 1, variation in the V_t in vehicle-treated animals was low, and variability between 2 consecutive PET scans (test–retest design) was approximately 10%. These data suggested that ^{18}F-UCB-H can be used to reproducibly quantify the availability of SV2A in vivo. Further studies with unlabeled UCB-H to block ^{18}F-UCB-H binding could further confirm the selectivity of ^{18}F-UCB-H for SV2A. The use of a test–retest experimental design allowed each animal to serve as its own internal control, making the percentage change in the V_t a useful measure of tracer displacement. A drawback of using a test–retest design with a tracer requiring an AIF is the degree of complexity introduced.

The use of a β-microprobe system for AIF determination made the full quantification of ^{18}F-UCB-H binding through kinetic modeling possible in the absence of a brain reference region. Tracer kinetic models based on estimation of the AIF from a reference region depend on the presence of a region devoid of specific tracer binding (*21*). The widespread distribution of SV2A in the brain (Fig. 2) precludes the use of such models. The accuracy of the β-microprobe–derived AIF relative to gold standard manual sampling was demonstrated previously (*12*). In the present study, the β-microprobe–derived AIF was used with a test–retest experimental design for the first time (to our knowledge). No adverse effects

TABLE 1
V_t in Controls ($n = 4$), Reproducibility of V_t, and Blocking of ^{18}F-UCB-H Binding by LEV

Brain region	V_t (mL/cm^3)*	Reproducibility of V_t†	Blocking of ^{18}F-UCB-H binding by LEV at‡: 0.1 mg/kg	1 mg/kg	10 mg/kg	100 mg/kg
Nucleus accumbens	10.9 ± 0.5	3.3 ± 15.0	−7.3 ± 1.4	−16.3 ± 7.1	−35.2 ± 20.4	−53.2 ± 9.0§
Amygdala	9.0 ± 0.3	3.9 ± 13.6	−8.7 ± 5.3	−16.0 ± 8.1	−33.0 ± 24.4	−49.0 ± 11.3§
Cerebellum	9.0 ± 0.2	2.2 ± 13.3	−7.4 ± 3.9	−15.6 ± 7.5	−30.2 ± 23.7	−43.8 ± 8.4‖
Cerebral cortex	9.4 ± 0.4	3.6 ± 12.8	−10.3 ± 6.0	−16.3 ± 8.4	−33.0 ± 20.5	−48.6 ± 9.2‖
Striatum	11.3 ± 0.5	3.3 ± 14.5	−7.6 ± 4.0	−17.1 ± 6.1	−35.1 ± 20.2	−53.5 ± 9.8§
Hippocampus	10.7 ± 0.5	3.3 ± 14.3	−9.2 ± 5.4	−15.7 ± 7.1	−34.1 ± 22.2	−52.6 ± 11.6§
Hypothalamus	9.9 ± 0.2	3.3 ± 13.2	−9.9 ± 1.3	−16.4 ± 7.7	−36.8 ± 23.3	−54.2 ± 9.0§
Medulla	8.5 ± 0.4	3.2 ± 12.1	−8.1 ± 4.5	−15.3 ± 7.1	−28.3 ± 17.5	−34.4 ± 9.2‖
Olfactory bulbs	9.0 ± 0.2	4.4 ± 12.0	−6.8 ± 2.5	−15.0 ± 7.1	−27.4 ± 22.3	−41.9 ± 9.2‖
Pons	8.2 ± 0.3	5.2 ± 12.4	−14.1 ± 0.2	−15.9 ± 5.4	−29.3 ± 8.7‖	−35.2 ± 11.7§
Septum	10.5 ± 0.4	4.6 ± 18.4	−6.9 ± 6.6	−16.9 ± 7.0	−33.4 ± 21.7	−50.8 ± 10.0‖
Thalamus	12.1 ± 0.6	2.5 ± 14.0	−10.8 ± 4.3	−16.1 ± 5.7	−36.2 ± 21.5	−55.8 ± 10.3§
Whole-brain average	9.8 ± 0.5	3.6 ± 13.1	−9.0 ± 4.6	−13.3 ± 3.3	−25.7 ± 28.0	−43.8 ± 4.7‖

*Determined by Logan graphic analysis and reported as mean ± SD.
†Determined as percentage difference in test–retest study and reported as mean ± SD.
‡Determined by Logan graphic analysis as percentage change in V_t in test–retest study and reported as mean ± SD.
§*P* value, determined by 1-way ANOVA and Tukey post hoc test, was less than 0.01.
‖*P* value, determined by 1-way ANOVA and Tukey post hoc test, was less than 0.05.

(i.e., signs of excessive pain, systemic infection, or poor wound healing) resulting from the removal of the femoral artery and femoral vein catheters after the test study were noted, and the use of the contralateral femoral artery and femoral vein for the retest study guaranteed patency for subsequent AIF measurement. Arterial blood samples taken during both studies confirmed that the in vivo metabolism of ^{18}F-UCB-H was consistent between scans (Fig. 4).

A drawback of the β-microprobe system for the measurement of AIF is low sensitivity. This drawback necessitates the injection of higher tracer activity (100–150 MBq) to ensure accurate counts in the tail of the AIF. In studies with low-specific-activity tracers and low levels of the target, this approach could lead to receptor saturation. However, SV2A is more abundantly expressed (maximum number of binding sites, 11 ± 2 pmol/mg of protein in rat cortex (*20*)) than several typical neurotransmitter receptor targets (*14,20,22,23*), and the radiochemical process yielded consistently high specific activities for ^{18}F-UCB-H. By comparing the injected mass of ^{18}F-UCB-H in the present study with the reported maximum number of binding sites of SV2A in the rat brain (*20*), we estimated that the occupancy of SV2A at the typical injected mass in the present study was less than 5%. The use of high tracer activity in microPET studies may lead to detector saturation and subsequent errors in quantification. Tests with a high-activity phantom in the Focus 120 scanner indicated that quantification was not compromised in the present study (data not shown), but we recommend that users test the performance of their scanners.

Measurement of the AIF in whole blood with the β-microprobe system necessitated correction of the measured AIF for metabolism in vivo. As shown in Figure 4, the metabolism of ^{18}F-UCB-H in vivo was highly reproducible and well fitted to a biexponential model. This model was used to correct the measured AIF after the application of a correction for the distribution of the tracer between plasma and whole blood over the study duration. Finally, the delay between the true tissue AIF and the measured external AIF was corrected by the inclusion of a delay parameter in the kinetic models.

In addition to its potential value in the study of epilepsy, ^{18}F-UCB-H could be of interest as a global measure of synaptic density. SV2 does not appear to affect vesicle formation, as synaptic morphology and vesicle density were not altered in SV2 knockout animals (*9,24,25*). These data suggested that SV2 could influence SV cycling. As this cycling is a continuous process within the presynaptic terminal, it could be postulated that reduced uptake of an SV2A PET tracer is a consequence of synaptic loss. Such a noninvasive measure of synaptic density could be of great value for the diagnosis of neurodegenerative disorders, including Alzheimer disease. At present, changes in synaptic density are only confirmed postmortem (*26,27*), and commonly used imaging techniques are generally limited to measures of neuronal or synaptic glucose metabolism and gray matter volume (*28*). Only studies with patient populations for whom postmortem follow-up is likely to be possible soon after PET will fully validate radiotracer-based measures of synaptic density, although PET scans with ^{18}F-UCB-H in patients with neurodegenerative disorders known to result in reduced synaptic density and in animal models may provide useful information.

CONCLUSION

To our knowledge, ^{18}F-UCB-H is the first reported PET tracer for SV2A. Our results indicated that ^{18}F-UCB-H is a suitable tracer for the assessment of SV2A density in vivo in rats. Dosimetry studies (*11*) indicated that ^{18}F-UCB-H can be used safely in humans, and an initial human study is planned. Further studies in animals and humans are needed to assess the value of ^{18}F-UCB-H for studying the pathophysiology of epilepsy and whether SV2A density represents a useful measure of synaptic density.

DISCLOSURE

The costs of publication of this article were defrayed in part by the payment of page charges. Therefore, and solely to indicate this fact, this article is hereby marked "advertisement" in accordance with 18 USC section 1734. This work was funded by the Walloon Region Public Private Partnership NEUROCOM, with University of Liège and UCB Pharma as partners. Florian Bretin is supported by Marie Curie Initial Training Network (MCITN) Methods in Neuroimaging under grant MC-ITN-238593. Mohamed Ali Bahri is a "logistical collaborator," and Alain Plenevaux is a senior research associate from FRS-FNRS Belgium. No other potential conflict of interest relevant to this article was reported.

ACKNOWLEDGMENTS

We acknowledge the valuable contributions from the reviewers during the submission process.

REFERENCES

1. Jahn R, Fasshauer D. Molecular machines governing exocytosis of synaptic vesicles. *Nature.* 2012;490:201–207.
2. Janz R, Sudhof TC, Hammer RE, Unni V, Siegelbaum SA, Bolshakov VY. Essential roles in synaptic plasticity for synaptogyrin I and synaptophysin I. *Neuron.* 1999;24:687–700.
3. Buckley K, Kelly RB. Identification of a transmembrane glycoprotein specific for secretory vesicles of neural and endocrine cells. *J Cell Biol.* 1985;100:1284–1294.
4. Crevecoeur J, Kaminski RM, Rogister B, et al. Expression pattern of synaptic vesicle protein 2 (SV2) isoforms in patients with temporal lobe epilepsy and hippocampal sclerosis. *Neuropathol Appl Neurobiol.* 2014;40:191–204.
5. Nowack A, Yao J, Custer KL, Bajjalieh SM. SV2 regulates neurotransmitter release via multiple mechanisms. *Am J Physiol Cell Physiol.* 2010;299:C960–C967.
6. Lynch BA, Lambeng N, Nocka K, et al. The synaptic vesicle protein SV2A is the binding site for the antiepileptic drug levetiracetam. *Proc Natl Acad Sci USA.* 2004;101:9861–9866.
7. Bajjalieh SM, Frantz GD, Weimann JM, McConnell SK, Scheller RH. Differential expression of synaptic vesicle protein 2 (SV2) isoforms. *J Neurosci.* 1994;14:5223–5235.
8. Janz R, Sudhof TC. SV2C is a synaptic vesicle protein with an unusually restricted localization: anatomy of a synaptic vesicle protein family. *Neuroscience.* 1999;94:1279–1290.
9. Janz R, Goda Y, Geppert M, Missler M, Sudhof TC. SV2A and SV2B function as redundant Ca_2^+ regulators in neurotransmitter release. *Neuron.* 1999;24:1003–1016.
10. Mercier J, Archen L, Bollu V, et al. Discovery of heterocyclic nonacetamide synaptic vesicle protein 2A (SV2A) ligands with single-digit nanomolar potency: opening avenues towards the first SV2A positron emission tomography (PET) ligands. *ChemMedChem.* 2014;9:693–698.
11. Bretin F, Warnock G, Bahri MA, et al. Preclinical radiation dosimetry for the novel SV2A radiotracer [^{18}F]UCB-H. *EJNMMI Res.* 2013;3:35.
12. Warnock G, Bahri MA, Goblet D, et al. Use of a beta microprobe system to measure arterial input function in PET via an arteriovenous shunt in rats. *EJNMMI Res.* 2011;1:13.
13. Logan J, Fowler JS, Volkow ND, et al. Graphical analysis of reversible radioligand binding from time-activity measurements applied to [*N*-^{11}C-methyl]-(−)-cocaine PET studies in human subjects. *J Cereb Blood Flow Metab.* 1990;10:740–747.

14. Gillard M, Fuks B, Michel P, Vertongen P, Massingham R, Chatelain P. Binding characteristics of [^{3}H]ucb 30889 to levetiracetam binding sites in rat brain. *Eur J Pharmacol.* 2003;478:1–9.
15. Motulsky HJ, Mahan LC. The kinetics of competitive radioligand binding predicted by the law of mass action. *Mol Pharmacol.* 1984;25:1–9.
16. Aerts J, Voccia S, Lemaire C, et al. Fast production of highly concentrated reactive [^{18}F] fluoride for aliphatic and aromatic nucleophilic radiolabelling. *Tetrahedron Lett.* 2010;51:64–66.
17. Aerts J, Otabashi M, Giacomelli F, et al. Radiosynthesis and first small animal microPET imaging of [^{18}F]UCB-H, a new fluorine-18 labelled tracer targeting synaptic vesicle protein 2A (SV2A): EANM Abstracts 2013. *Eur J Nucl Med Mol Imaging.* 2013;40:S89–S565.
18. Bahri MA, Plenevaux A, Warnock G, Luxen A, Seret A. NEMA NU4-2008 image quality performance report for the microPET Focus 120 and for various transmission and reconstruction methods. *J Nucl Med.* 2009;50:1730–1738.
19. Weber B, Späth N, Wyss M, et al. Quantitative cerebral blood flow measurements in the rat using a beta-probe and H2 15O. *J Cereb Blood Flow Metab.* 2003;23:1455–1460.
20. Gillard M, Fuks B, Leclercq K, Matagne A. Binding characteristics of brivaracetam, a selective, high affinity SV2A ligand in rat, mouse and human brain: relationship to anti-convulsant properties. *Eur J Pharmacol.* 2011;664:36–44.
21. Lammertsma AA, Hume SP. Simplified reference tissue model for PET receptor studies. *Neuroimage.* 1996;4:153–158.
22. Gould GG, Brooks BW, Frazer A. [^{3}H]citalopram binding to serotonin transporter sites in minnow brains. *Basic Clin Pharmacol Toxicol.* 2007;101:203–210.
23. Tanibuchi Y, Wu J, Toyohara J, Fujita Y, Iyo M, Hashimoto K. Characterization of [^{3}H]CHIBA-1001 binding to alpha7 nicotinic acetylcholine receptors in the brain from rat, monkey, and human. *Brain Res.* 2010;1348:200–208.
24. Crowder KM, Gunther JM, Jones TA, et al. Abnormal neurotransmission in mice lacking synaptic vesicle protein 2A (SV2A). *Proc Natl Acad Sci USA.* 1999;96:15268–15273.
25. Morgans CW, Kensel-Hammes P, Hurley JB, et al. Loss of the synaptic vesicle protein SV2B results in reduced neurotransmission and altered synaptic vesicle protein expression in the retina. *PLoS ONE.* 2009;4:e5230.
26. Padurariu M, Ciobica A, Mavroudis I, Fotiou D, Baloyannis S. Hippocampal neuronal loss in the CA1 and CA3 areas of Alzheimer's disease patients. *Psychiatr Danub.* 2012;24:152–158.
27. Yang Y, Mufson EJ, Herrup K. Neuronal cell death is preceded by cell cycle events at all stages of Alzheimer's disease. *J Neurosci.* 2003;23:2557–2563.
28. Johnson KA, Fox NC, Sperling RA, Klunk WE. Brain imaging in Alzheimer disease. *Cold Spring Harb Perspect Med.* 2012;2:a006213.